Preprints of the 5th IFAC Symposium on Mechatronic Systems
Marriott Boston Cambridge
Cambridge, MA, USA, September 13-15, 2010

MECHATRONICS2010-128

High Performance Nanopositioning with Integrated Strain and Force Feedback ⋆

Andrew J. Fleming * **Kam K. Leang** **

* *School of Electrical Engineering and Computer Science, University of Newcastle, Callaghan, NSW 2308, Australia (email: andrew.fleming@newcastle.edu.au)*
** *Mechanical Engineering, University of Nevada, Reno, NV 89557 (email: kam@unr.edu)*

Abstract: This paper presents a new sensor arrangement and feedback controller for hysteresis, creep and vibration in piezoelectric actuators. A force and strain sensor is combined to provide both extremely low noise and high stability. The proposed technique is demonstrated on a nanopositioning platform with a range of 10 μm and a resonance frequency of 2.4 kHz. In closed-loop, the controller damps the resonance by 33 dB and provides a tracking bandwidth of 1.8 kHz. Excellent tracking of a 130 Hz triangular reference and reduction of hysteresis to 0.46% at 10 Hz is also demonstrated. Closed-loop positioning noise was approximately 0.67 nm peak-to-peak, or 0.0067% of the 10 μm range.

Keywords: Nanopositioning, Motion Control, Hysteresis, Creep, Force Feedback, Sensor Fusion, Piezoelectric Actuators, Position Sensing

1. INTRODUCTION

Due to their high stiffness, compact size and effectively infinite resolution, piezoelectric actuators are universally employed in a wide range of scientific and industrial applications. However, piezoelectric actuators also exhibit a significant amount of hysteresis over large ranges and creep at low-frequencies [Adriaens et al. (2000); Devasia et al. (2007)]. These effects can cause tracking error in excess of 20%. As a result, many applications require some form of feedback or feedforward control to reduce or eliminate non-linearity [Leang and Devasia (2007); Croft et al. (2001)].

A common technique for control of piezoelectric actuated systems is sensor-based feedback control with an integral or proportional-integral controller. This approach is simple, robust to modeling error, and effectively reduces non-linearity at low-frequencies. However, the bandwidth of such systems is severely limited by low gain-margin [Leang and Devasia (2007)]. It can be shown that the maximum closed-loop bandwidth with a basic integral controller is equal to the product of twice the damping ratio ξ and natural frequency ω_n [Fleming (2010)], that is,

$$\text{max. closed-loop bandwidth} < 2\omega_n\xi. \quad (1)$$

This is a severe limitation as the damping ratio is usually on the order of 0.01, so the maximum closed-loop bandwidth is less than 2% of the resonance frequency. Techniques aimed at improving the closed-loop bandwidth are based on either inversion of resonant dynamics using a notch filter[Abramovitch et al. (2008)] or a damping controller [Fleming and Moheimani (2006); Aphale et al. (2008); Fleming et al. (2010); Sebastian et al. (2008)]. Damping controllers are less sensitive to variations in resonance frequency than inversion based controllers but an integral tracking loop is still required. This inevitably results in low stability margin and instability if the resonance frequency is sufficiently reduced. In addition, the greater bandwidth of damping and inversion based controllers increases the amount of positioning noise.

In this work, a new technique is presented for control of hysteresis, creep and vibration in piezoelectric actuated systems. The proposed technique utilizes a resistive strain gage and piezoelectric force sensor to estimate displacement. The piezoelectric force sensor exhibits extremely low noise at frequencies in the Hz range and above but cannot measure static displacement and is prone to drift. To eliminate these low-frequency errors, the strain gage signal is substituted at low frequencies. In contrast to standard capacitive, inductive and optical displacement sensors, the proposed scheme can be integrated into the actuator which minimizes parts count and overall system cost.

In the following Section a nanopositioning system is described for demonstration of the proposed technique. This is followed by an introduction to strain and piezoelectric force sensors in Sections 3 and 4. Section 4 also contains the derivation of an electromechanical model and a review of the recently introduced technique of force-feedback position control [Fleming (2010)]. This technique is extended in Section 5 for use with complementary strain and force sensors. Due to the system properties, a simple integral controller can provide excellent tracking and damping performance with guaranteed stability. This technique is demonstrated in Section 6. Conclusions are drawn in Section 7.

⋆ This research was supported by the Australian Research Council (DP0666620) and in part by the Nevada NASA Space Grant Consortium.

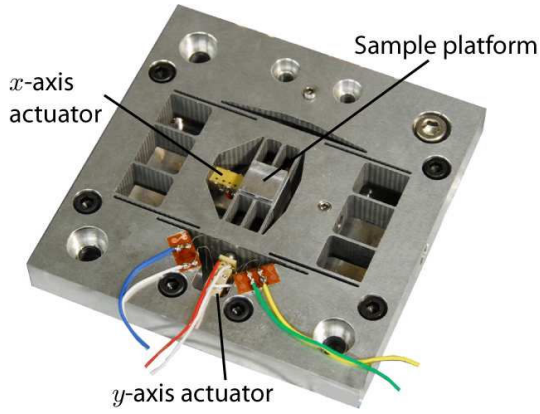

Fig. 1. High-speed nanopositioning platform with strain and force sensors fitted to the y-axis actuator.

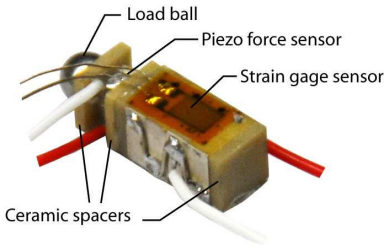

Fig. 2. A piezoelectric actuator with integrated strain and force sensors. The strain sensors are bonded to the front and back surface while the force sensor is a small piezoelectric stack placed between the actuator and load ball. The load half-ball is used to eliminate the transmission of torsion and bending moments to the force sensor and moving platform.

2. EXPERIMENTAL SYSTEM

Although the technique of strain and force feedback is applicable to a wide range of mechatronic systems, in this work, the proposed controller is applied to the nanopositioning platform pictured in Figure 1. This platform is designed for high-bandwidth applications such as video-speed scanning probe microscopy [Ando et al. (2005); Schitter et al. (2007); Humphris et al. (2005); Rost et al. (2005)]. The platform develops approximately 10 μm of travel in the lateral scan axes and 4 μm travel in the vertical direction. As the vertical and x-axes are physically small with low mass, the resonance frequencies are greater than 10 kHz. However, due to the large y-axis mass, the resonance frequency in this direction is only 2.4 kHz. As this axis is required to follow triangular trajectories of up to 100 Hz, compensation is required to eliminate oscillation and reduce non-linearity. The technique of strain and force feedback will be applied to achieve high-performance tracking with simplicity, low-cost and high robustness.

The actuator used to drive the y-axis is pictured in Figure 2. It comprises of a 10 mm Noliac SCMAP07 actuator connected serially to a 2 mm Noliac CMAP06 stack force sensor. The ceramic spacers provide a robust bonding surface between the two stacks and minimize the measurement error due to Poisson coupling. This error is caused by contraction of the stack body during elongation. If the sensor bonded directly on to the actuator, this contraction is erroneously measured and produces an effect opposite in polarity to the applied force. A further discussion of Poisson coupling and methods to eliminate it can be found in Fleming (2010). In addition to the force sensor, there are also two resistive strain sensors attached to the top and bottom surface of the actuator. A full description of the strain gages, instrumentation, and force sensor are provided in Sections 3 and 4. A Kaman inductive position sensor (SMU9000-15N) was also used to measure the frequency and time domain displacement of the system. These open-loop responses are plotted in Section 6.

The actuator was driven with a Piezodrive PDL200 linear amplifier. With the 330 nF actuator capacitance, the PDL200 provides a bandwidth of approximately 22 kHz.

3. RESISTIVE STRAIN FEEDBACK

Resistive strain gages are a low-cost sensor option for control of piezoelectric actuators. They are often integrated into actuators by the manufacturer for position feedback. Strain sensors can also be retrofitted to other actuators by bonding the sensor to the actuator surface. Two other nanopositioning applications that utilize resistive strain feedback can be found in Schitter et al. (2008) and Dong et al. (2007).

Resistive strain gages are constructed from a thin layer of conducting foil laminated between two insulating layers. With a zig-zag conductor pattern, strain gages can be designed for high sensitivity in only one direction, e.g. elongation. As a strain gage is elongated, the resistance increases proportionally. The change in resistance per unit strain is known as the gage factor GF defined by

$$\mathrm{GF} = \frac{\Delta R / R_G}{\epsilon}, \tag{2}$$

where ΔR is the change in resistance from the nominal value R_G for a strain ϵ. As the gage factor is typically in the order of 1 or 2, the change is resistance is similar in magnitude to the percentage of strain. For a piezoelectric transducer with a maximum strain of approximately 0.1%, the change in resistance will also be around 0.1%. This small variation requires a bridge circuit for accurate measurement.

In Figure 2, the piezoelectric actuator described in Section 2 is pictured with a strain gage bonded to each of the two non-electrode sides. The strain gages are Omega SGD-3/350-LY13 gages, with a nominal resistance of 350 Ω and package dimensions of 7×4 mm.

The two strain gages are wired into a full bridge circuit completed by two dummy 350 Ω wire wound resistors and excited by a 5 Volt DC source. The differential bridge voltage $(V^+ - V^-)$ is acquired and amplified by a Vishay Micro-Measurements 2120B strain gage amplifier. As the circuit is a half-bridge, the measured voltage is

$$V_s = \frac{A_v V_b}{2} \left(\frac{\Delta R}{R_G + \Delta R/2} \right), \tag{3}$$

where A_v=2000 is the differential gain and V_b=5V is the excitation voltage. By substituting (2) into (3) and neglecting the small bridge non-linearity, the measured voltage is proportional to the strain ϵ and displacement d by

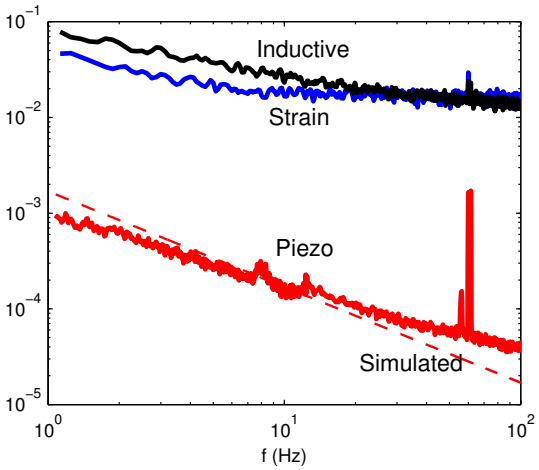

Fig. 3. The noise density of the inductive, resistive strain, and piezoelectric force sensor, all scaled to nm/$\sqrt{\text{Hz}}$. The simulated noise of the piezoelectric force sensor is also plotted as a dashed line.

$$V_s = \text{GF}\frac{1}{2}A_v V_b \epsilon \tag{4}$$

$$V_s = \text{GF}\frac{1}{2L}A_v V_b d, \tag{5}$$

where L is the actuator length. With a gage factor of 1, the position sensitivity of the strain sensor will be 0.5 V/μm which implies a full scale voltage of 5 V for the maximum strain of 10 μm.

By calibrating the strain gage output with the inductive sensor, the experimental sensitivity was found to be 0.3633 V/μm.

The noise density of the strain signal (scaled to nm) is plotted in Figure 3. The sensor exhibits a constant noise density of approximately 20 pm/$\sqrt{\text{Hz}}$ and a 1/f noise corner frequency of around 10 Hz. This is comparable to the inductive sensor which has a range of 200 μm. However, for an inductive or capacitive sensor with a range of 10 μm, the expected noise density would be only 1 pm/$\sqrt{\text{Hz}}$, which is an order of magnitude less than the resistive strain gage. Hence, strain gages are rarely used in systems designed for high resolution. If they are utilized in such systems, the closed-loop bandwidth must be severely restrained. For example, with a noise density of 20 pm/$\sqrt{\text{Hz}}$, the closed-loop bandwidth must be less than 22 Hz to achieve a peak-to-peak noise of 1 nm (assuming a Gaussian distribution and first-order response). To overcome this difficultly, an ultra-low noise force sensor is described in the following section.

4. FORCE FEEDBACK

Force feedback was recently proposed in Fleming (2010) as a new technique for vibration control and linearization of nanopositioning systems. Rather than using a direct position sensor, this technique uses a measurement of the actuator load force illustrated in Figure 4(a). Since the displacement of the load system is proportional to applied force at low-frequencies, the load force can be used to indirectly control position.

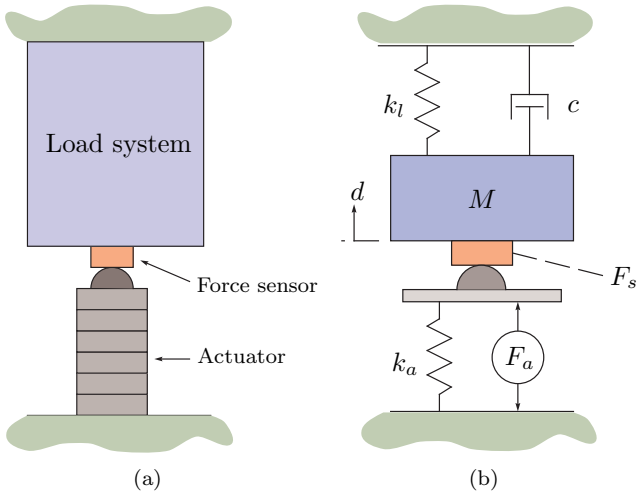

Fig. 4. A piezoelectric actuator driving a load system (a). The mechanical equivalent diagram with a single-degree-of-freedom load system (b).

Although the load force F_s can be measured in a number of ways, in this application it is desirable to minimize the additional mass and compliance associated with the sensor. In such scenarios, piezoelectric transducers are an excellent choice. They provide high sensitivity and bandwidth with low-noise at high frequencies. In Figure 2, a small Noliac CMAP06 stack actuator is glued to the end of the main actuator for use as a force sensor. Other types of piezoelectric force sensor include discrete plate sensors and integrated stack sensors [Fleming (2010)]. The sensitivity and characteristics of piezoelectric force sensors are discussed in the following two subsections.

4.1 Piezoelectric actuator and sensor modeling

It has been shown previously that a piezoelectric actuator can be modeled as a force generator F_a and stiffness k_a [Fleming (2010)]. This representation is shown in Figure 4(b). The generated force and associated spring constant are

$$F_a = d_{33} n k_a V_a, \qquad k_a = \frac{c^E A}{L}, \tag{6}$$

where d_{33} is the piezoelectric charge constant, n is the number of layers, V_a is the applied voltage, c^E is Young's modulus of elasticity, A is the cross-sectional area, and L is the actuator length. The ratio of developed force to applied voltage is $d_{33} n k_a$ Newtons per Volt. In the following, this constant will be denoted g_a where

$$F_a = g_a V_a \quad \text{and,} \quad g_a = d_{33} n k_a.$$

Piezoelectric actuators can also be used as force sensors. If the transducer electrodes are left open-circuit or connected to a high impedance buffer, the generated charge is deposited on the transducers internal capacitance. The open-circuit voltage of a piezoelectric force sensor is

$$V_s = \frac{n d_{33}}{C} F_s, \tag{7}$$

where C is the transducer capacitance defined by $C{=}n\epsilon_T A/h$ and A, h and ϵ_T are the area, layer thickness and dielectric permittivity under constant stress. The scaling factor between force and measured voltage is $\frac{n d_{33}}{C}$

Volts per Newton. In the following, this sensor constant will be denoted g_s, where

$$V_s = g_s F_s, \quad \text{and} \quad g_s = \frac{n d_{33}}{C}. \tag{8}$$

4.2 Force sensor characteristics and noise

The experimentally measured noise density of the piezoelectric force sensor is plotted in Figure 3. The predicted noise density based on the opamp current noise density and capacitance is also plotted. The sensor has a capacitance is 30 nF, and the voltage buffer (OPA606) has a noise density of 2 fA/$\sqrt{\text{Hz}}$.

In Figure 3 the superior noise performance of the piezoelectric sensor is evident. The noise density is more than 2 orders of magnitude lesser than the strain and inductive sensors at 100 Hz. The noise density also continues to reduce at higher frequencies. However, at low-frequencies the noise of the piezoelectric force sensor will eventually surpass the other sensors. As the noise density is equivalent to an integrator excited by white noise, the measured voltage will drift around at low frequencies.

In addition to noise, piezoelectric force sensors are also limited by dielectric leakage and finite buffer impedance at low-frequencies. The induced voltage V_p is high-pass filtered by the internal transducer capacitance C and the leakage resistance R. The cut-off frequency is

$$f_{hp} = \frac{1}{2\pi RC} \text{ Hz}. \tag{9}$$

The buffer circuit used in this work has an input impedance of 100 MΩ, this results in a low-frequency cut-off of 0.05 Hz. To avoid a phase lead of more than 6 degrees, the piezoelectric force sensor cannot be used to measure frequencies less than 0.5 Hz.

4.3 Mechanical dynamics

The simplified model of a single-degree-of-freedom positioning system is shown in Figure 4(b). The model contains two components: the actuator, modeled as a force generator F_a and stiffness k_a; and the load system, modeled as a mass M and stiffness k_l with damping c. The actuator mass is assumed to be negligible. The displacement of the load system d can be found by applying Newton's second law,

$$M\ddot{d} = F_a - k_a d - k_l d - c\dot{d}, \tag{10}$$

As the actuator and load stiffness are mechanically in parallel. The total stiffness k experienced by the load mass is the sum of k_a and k_l. That is, $k = k_a + k_l$. The equation of motion is then

$$M\ddot{d} + kd + c\dot{d} = F_a, \tag{11}$$

and the transfer function from actuator force F_a to platform displacement d is

$$\frac{d}{F_a} = \frac{1}{Ms^2 + cs + k}. \tag{12}$$

Including the actuator gain, the transfer function from applied voltage to displacement can be written

$$G_{dVa} = \frac{d}{V_a} = \frac{g_a}{Ms^2 + cs + k} \tag{13}$$

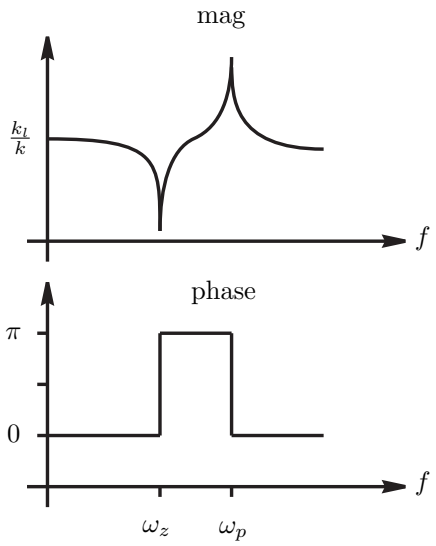

Fig. 5. Magnitude and phase response of F_s/F_a (15)

The load force F_s is also of interest, this can be related to the actuator force F_a by summing the forces acting on the force sensor,

$$F_a = k_a d - F_s. \tag{14}$$

This results in the following transfer function between the applied force F_a and measured force F_s,

$$\frac{F_s}{F_a} = 1 - k_a \frac{d}{F_a} \tag{15}$$

$$= \frac{Ms^2 + cs + k_l}{Ms^2 + cs + k}. \tag{16}$$

By including the actuator and sensor gains g_a and g_s, the system transfer function from the applied voltage to measured voltage can be found,

$$G_{VsVa} = \frac{V_s}{V_a} = g_a g_s \frac{Ms^2 + cs + k_l}{Ms^2 + cs + k}. \tag{17}$$

4.4 System poles and zeros

This transfer function G_{VsVa} (17) consists of a pair of resonant poles and zeros at frequencies ω_z and ω_p,

$$\omega_z = \sqrt{\frac{k_l}{M}}, \quad \omega_p = \sqrt{\frac{k}{M}} = \sqrt{\frac{k_a + k_f}{M}}. \tag{18}$$

The frequency of the system zeros will always be lower than the poles. This characteristic is shown in the frequency response of F_s/F_a in Figure 5. For systems with multiple degrees-of-freedom, it can be shown that the zero-pole pattern repeats for each resonance mode. This is discussed in more detail in Section 5.1.

4.5 Integral Force Feedback (IFF)

The feedback diagram of an integral force feedback controller is shown in Figure 6. The loop consists of the plant G_{VsVa} and an integral controller

$$C(s) = \frac{\alpha}{s}. \tag{19}$$

A key property of the system G_{VsVa} is that the phase response lies between 0 and 180 degrees. This is a general feature of flexible structures with a collocated actuator and

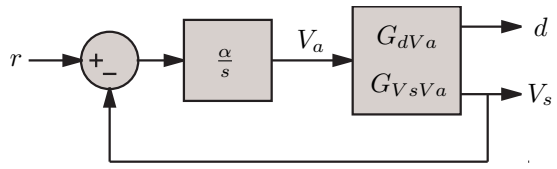

Fig. 6. The system G_{VsVa} controlled by an Integral Force Feedback (IFF) controller $C(s)=\frac{\alpha}{s}$

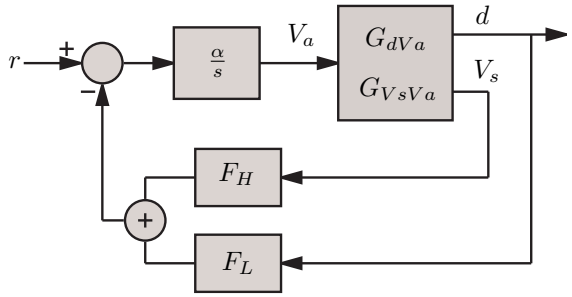

Fig. 7. Dual sensor feedback loop that utilizes a strain gage measurement below 10 Hz and the piezoelectric force measurement above 10 Hz.

force measurement [Preumont (2006)]. Another unique property of such systems is that integral control can be applied directly. This is due to the phase characteristics of the loop-gain. As the integral controller has a constant phase lag of 90 degrees, the total loop-gain phase ($\angle C(j\omega)G_{VsVa}(j\omega)$) lies between -90 and 90 degrees. This implies that the closed-loop system has an infinite gain-margin and phase-margin of 90 degrees. The robustness and simplicity are two outstanding properties of systems with integral force feedback.

A solution for the optimal feedback gain α for maximum damping has already been derived in Preumont (2006). These results were adapted for the system considered here in reference [Fleming (2010)]. Assuming the system damping is small, the optimal feedback gain $\alpha^\star$ is

$$\alpha^\star = \frac{\omega_p\sqrt{\omega_p/\omega_z}}{g_s g_a}. \tag{20}$$

Additional expressions for the maximum closed-loop damping and pole locations can be found in Fleming (2010). In practice, where only an identified model may be available, the optimal gain $\alpha^\star$ can be found numerically from the root-locus. This approach is taken in Section 6.

The closed-loop transfer functions from the reference voltage to the displacement and measured force, $\widehat{G_{dr}}$ and $\widehat{G_{V_s r}}$, are

$$\widehat{G_{dr}} = \frac{CG_{dVa}}{1+CG_{VsVa}}. \tag{21}$$

$$\widehat{G_{V_s r}} = \frac{CG_{VsVa}}{1+CG_{VsVa}}. \tag{22}$$

With integral force feedback the position is regulated indirectly by controlling the load force F_s. The closed-loop position sensitivity can be determined from (21) to be $1/g_s k_l$ meters per Volt.

5. STRAIN AND FORCE FEEDBACK

In Section 3 resistive strain gages were discussed as a method for position control of piezoelectric actuators. It was concluded that strain gages are too noisy for high-bandwidth positioning applications. In contrast, piezoelectric force sensors have excellent noise performance at frequencies in the Hz range and above. In addition, the use of a force sensor results in a system that can be easily controlled with excellent bandwidth and stability margins.

To overcome the noise and phase-lead exhibited by the piezoelectric sensor at low frequencies the strain gage can be utilized as a complementary sensor. Such an arrangement is illustrated in Figure 7. This control loop is similar to Figure 6 except for the additional complementary filters F_H and F_L. These complementary filters substitute the displacement measurement d for V_s at frequencies below the crossover frequency f_c. As the force measurement contains a parasitic high-pass filter at 0.05 Hz, f_c is chosen to be 10 Hz. At this frequency the phase error of the force sensor is less than 0.5 degrees. The simplest choice of complementary filters are

$$F_H = g_H\frac{s}{s+2\pi f_c}, \text{ and } F_L = g_L\frac{2\pi f_c}{s+2\pi f_c}. \tag{23}$$

where g_H and g_L are gains used to equate the sensitivity of d and V_s. In practice, it is convenient to choose g_H and g_L so that the sensitivity from V_a to each sensor signal is unity. This approach is taken in the experimental results.

If the gains g_H and g_L are included in G_{VsVa} and G_{dVa} respectively, the closed-loop response $\widehat{G_{dr}}$ is

$$\widehat{G_{dr}} = \frac{G_{dVa}C}{1+CG_{VsVa}}. \tag{24}$$

As this control loop is unconditionally stable, there is no restriction on the controller gain. However, α was chosen in the previous section to provide optimal damping performance, this value should be retained. Further increases in α are not productive as the disturbance rejection at the resonance frequency will degrade.

As the piezoelectric sensor noise is negligible compared to the strain gage, and the crossover frequency f_c is significantly less than the closed-loop bandwidth, the closed-loop position noise density of the dual sensor controller can be approximated by

$$\widehat{N_d}(\omega) = |F_L(j\omega)|\, N_d(\omega), \tag{25}$$

where $\widehat{N_d}$ is the closed-loop noise density and $N_d(\omega)$ is the noise density of the strain gage scaled to meters. Advantageously, the strain signal is filtered by F_L which has a much lower bandwidth than the complimentary sensitivity function, hence a large saving in position noise is realized.

If we assume that $N_d(\omega)$ is a constant N_d, the standard deviation σ (RMS value) of the positioning noise is

$$\sigma = N_d\sqrt{3.14 f_c}, \tag{26}$$

where the factor 3.14 is the effective noise bandwidth for a first order system. For the strain gages discussed in Section 3, the noise density is approximately 20 pm/$\sqrt{\text{Hz}}$, this implies a positioning noise of 0.11 nm RMS, and a 6σ peak-to-peak noise of approximately 0.67 nm.

5.1 Higher-order modes

So far, only a single-degree-of-freedom system has been considered. Although this is appropriate for modeling the first resonance mode, it does not capture the higher-order modes that occur in distributed mechanical systems. However, such higher order modes are not problematic as they do not disturb the zero-pole ordering of the transfer function from applied actuator voltage to the measured force.

In Preumont et al. (2007) it is shown that the transfer function of a generalized mechanical system with a discrete piezoelectric transducer and collocated force sensor is guaranteed to exhibit zero-pole ordering. That is, the transfer function G_{VsVa} will always exhibit zero-pole ordering. As the zero-pole ordering of the system is guaranteed, it follows that the controller discussed in Section 4.5 will also guarantee the stability of systems with multiple modes. The zero-pole ordering of an experimental system with multiple modes, and its successful control using integral force feedback was reported in Fleming (2010).

6. EXPERIMENTAL RESULTS

As the integral force feedback controller has only one parameter, an approximately optimal gain can be found from only frequency response data. However, to plot the closed-loop pole locations and find a numerically optimal gain, a model is required. For this purpose, a second-order single-input two-output model was procured using the frequency domain subspace techniqueThe open-loop data used to procure the model is plotted in Figure 8.

Using the root-locus, the optimal feedback gain was found to be α=7700. With this gain, the controller was implemented on an electronics board designed to implement all of the functions required by a force feedback system . This includes a high-impedance buffer for the force sensor, the complementary filters, and the controller transfer function.

The experimental closed-loop frequency responses are plotted in Figure 8. The closed-loop responses exhibit excellent damping performance (-33 dB) and a closed-loop positioning bandwidth of 1.8 kHz. This is exceptional considering that the open-loop resonance frequency is 2.4 kHz. Also plotted are the simulated closed-loop frequency responses which closely agree with experimental results.

In Figure 10 the time domain performance of the force feedback controller is demonstrated by comparing the open- and closed-loop response to a 130 Hz triangle wave. The controller effectively eliminates oscillation and reduces the tracking error from 45 nm in open-loop to 6.7 nm in closed-loop. Due to the integral tracking action and wide feedback bandwidth, the controller is also effective at reducing dynamic hysteresis. In Figure 11, the 8.5% error due to hysteresis in open-loop is reduced to 0.46% in closed-loop. It is also of interest to examine the closed-loop response to creep non-linearity. As the control-loop gain at frequencies where creep occurs is extremely large, the open-loop error of 9.7% after 50 seconds is no longer measurable in closed-loop.

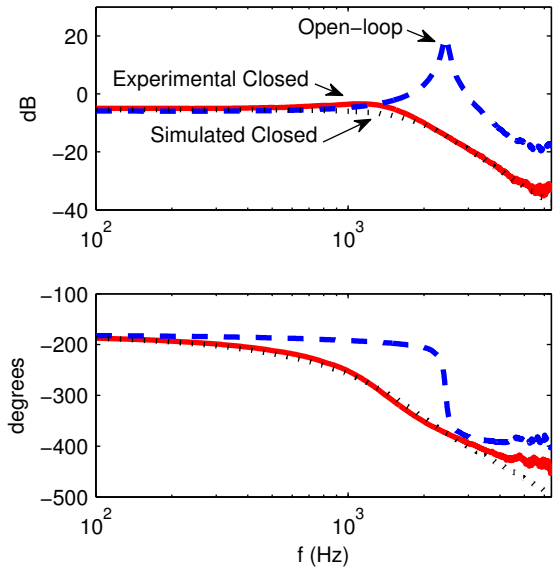

(a) Displacement G_{dr} (μm/V)

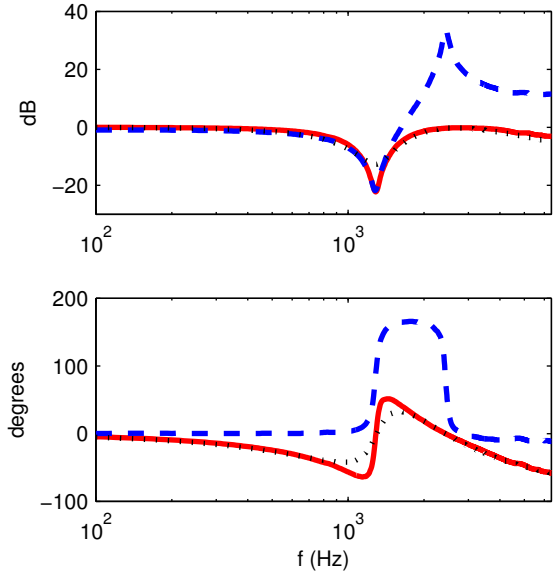

(b) Force G_{V_sr} (V/V)

Fig. 8. The experimental open- and closed-loop frequency response (dashed and solid line) from the applied voltage to the resulting displacement and sensor voltage. The simulated closed-loop response is also plotted (dotted line).

7. CONCLUSIONS

This paper presents a new low-cost sensing and feedback scheme for reduction of creep, hysteresis and vibration in piezoelectric actuated systems. The technique of strain and force feedback utilizes a resistive strain gage and piezoelectric force sensor to measure displacement. A benefit of piezoelectric sensors is that they exhibit extremely low noise at frequencies in the Hz range and above. However, below 1 Hz, dielectric leakage introduces phase-lead, and current noise results in slow random drift. To eliminate these low-frequency errors, the strain gage signal is substi-

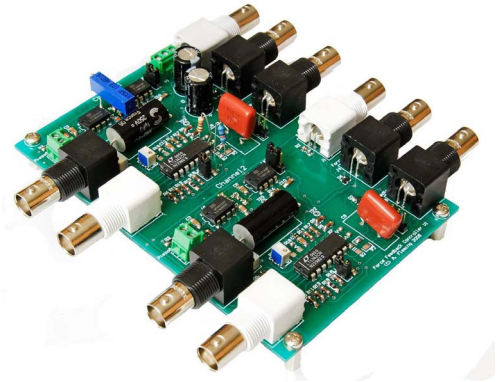

Fig. 9. A two channel controller board containing high-impedance buffers, complementary filters, and two force feedback controllers

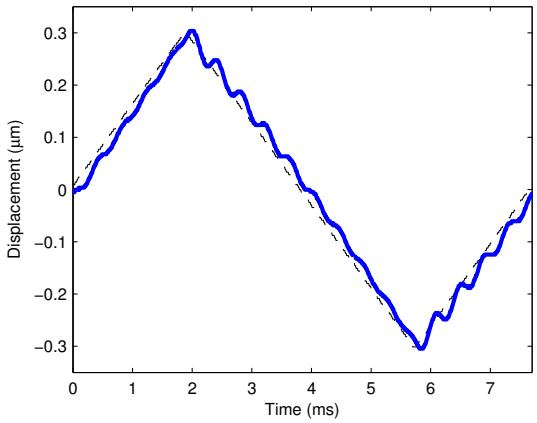

(a) Open-loop

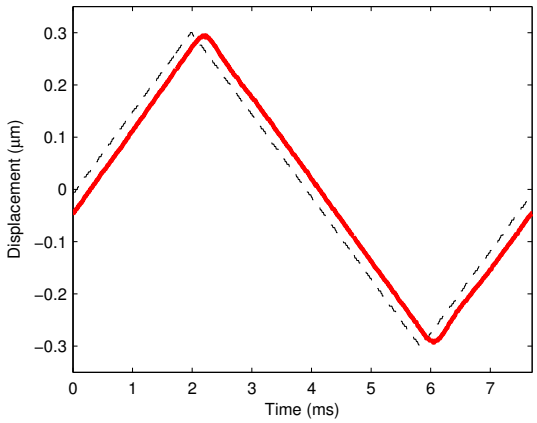

(b) Closed-loop

Fig. 10. The open- and closed-loop response to a 600 nm peak-to-peak 130 Hz triangle wave. The RMS deviation from linear over a half period was 10 nm RMS in open-loop and 1.9 nm RMS in closed-loop. The maximum peak-to-peak error over 90% of a half period was 45 nm in open-loop and 6.7 nm in closed-loop.

tuted at low frequencies. The strain gage and piezoelectric sensor signals are combined into a displacement estimate with a pair of first-order complementary filters. The resulting signal exhibits the low noise of a piezoelectric sensor and the stability of a resistive strain gage.

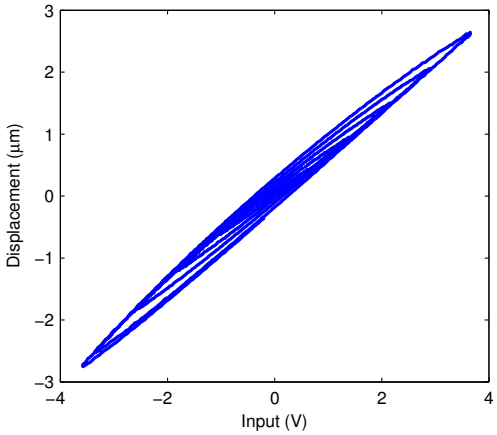

(a) Open-loop

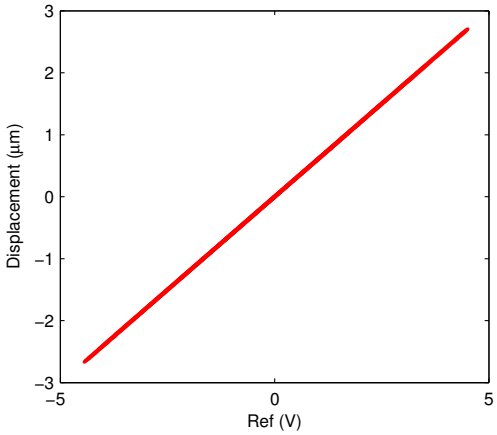

(b) Closed-loop

Fig. 11. The open- and closed-loop response of the system to a 10 Hz sine-wave ramped from 0 V to 150 V peak-to-peak. The maximum error due to hysteresis is reduced from 460 nm (8.5%) in open-loop to 25 nm (0.46%) in closed-loop.

In addition to low noise, another benefit of the piezoelectric force sensor is the zero-pole ordering of the transfer function from applied actuator voltage to measured force. This allows a simple integral controller to provide excellent tracking and damping performance with guaranteed stability.

The proposed technique of strain and force feedback was demonstrated on a high-speed nanopositioning platform. Due to simplicity, the controller was easily implemented with an analog circuit. The closed-loop frequency response demonstrated a 33 dB damping of the resonance peak and a closed-loop bandwidth of 1.8 kHz which is close to the open-loop resonance frequency of 2.4 kHz. In the time domain, excellent tracking of a 130 Hz triangle wave was achieved and hysteresis was reduced from 8.5% to 0.46% at 10 Hz. Although the strain gage contributes the majority of closed-loop positioning noise, the bandwidth of this signal is only 10 Hz. This resulted in a closed-loop noise of approximately 0.67 nm peak-to-peak which is 0.0067% of the 10 μm range.

Due to the low-cost of strain gages and piezoelectric sensors, and the simplicity of implementation, these results

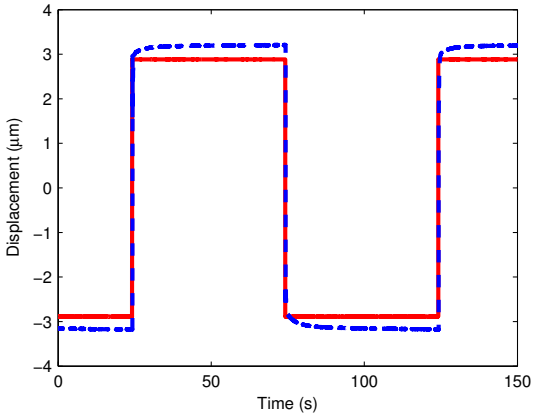

Fig. 12. The creep behavior exhibited by the actuator in open-loop (dashed line) and closed-loop (solid line). The input was a 196 V square with a period of 100 s. In open-loop, the error due to creep was 560 nm peak-to-peak or 9.7% of the peak-to-peak displacement. Due to the high control gain at low-frequencies, creep was not detectable in closed-loop.

were achieved at a fractional cost of a traditional inductive or capacitive displacement sensor. Future work involves the inclusion of a feedforward controller to extend the bandwidth beyond the first resonance frequency.

ACKNOWLEDGEMENTS

The authors gratefully acknowledge Brian J. Kenton for designing the nanopositioning system shown in Fig. 1.

REFERENCES

Abramovitch, D.Y., Hoen, S., and Workman, R. (2008). Semi-automatic tuning of PID gains for atomic force microscopes. In *Proc. American Control Conference*, 2684–2689. Seattle, WA.

Adriaens, H.J.M.T.A., W. L. de Koning, and Banning, R. (2000). Modeling piezoelectric actuators. *IEEE/ASME Transactions on Mechatronics*, 5(4), 331–341.

Ando, T., Kodera, N., Uchihashi, T., Miyagi, A., Nakakita, R., Yamashita, H., and Matada, K. (2005). High-speed atomic force microscopy for capturing dynamic behavior of protein molecules at work. *e-Journal of Surface Science and Nanotechnology*, 3, 384–392.

Aphale, S.S., Bhikkaji, B., and Moheimani, S.O.R. (2008). Minimizing scanning errors in piezoelectric stack-actuated nanopositioning platforms. *IEEE Transactions on Nanotechnology*, 7(1), 79–90.

Croft, D., Shed, G., and Devasia, S. (2001). Creep, hysteresis, and vibration compensation for piezoactuators: atomic force microscopy application. *ASME J. Dyn. Syst., Meas., and Control*, 123, 35–43.

Devasia, S., Eleftheriou, E., and Moheimani, S.O.R. (2007). A survey of control issues in nanopositioning. *IEEE Transactions on Control Systems Technology*, 15(5), 802–823.

Dong, W., Sun, L.N., and Du, Z.J. (2007). Design of a precision compliant parallel positioner driven by dual piezoelectric actuators. *Sensors and Actuators A*, 135(1), 250–256.

Fleming, A.J. (2010). Nanopositioning system with force feedback for high-performance tracking and vibration control. *IEEE Transactions on Mechatronics*, 15(3), 433–447.

Fleming, A.J., Aphale, S.S., and Moheimani, S.O.R. (2010). A new method for robust damping and tracking control of scanning probe microscope positioning stages. *IEEE Transactions on Nanotechnology, In Press*.

Fleming, A.J. and Moheimani, S.O.R. (2006). Sensorless vibration suppression and scan compensation for piezoelectric tube nanopositioners. *IEEE Transactions on Control Systems Technology*, 14(1), 33–44.

Humphris, A.D.L., Miles, M.J., and Hobbs, J.K. (2005). A mechanical microscope: high-speed atomic force microscopy. *Applied Physics Letters*, 86, 034106(1–3).

Leang, K.K. and Devasia, S. (2007). Feedback-linearized inverse feedforward for creep, hysteresis, and vibration compensation in AFM piezoactuators. *IEEE Transactions on Control Systems Technology*, 15(5), 927–935.

Preumont, A. (2006). *Mechatronics, Dynamics of electromechanical and piezoelectric systems*. Springer.

Preumont, A., de Marneffe, B., Deraemaeker, A., and Bossens, F. (2007). The damping of a truss structure with a piezoelectric transducer. *Computers and Structures*, 86, 227–239.

Rost, M.J., Crama, L., Schakel, P., van Tol, E., van Velzen-Williams, G.B.E.M., Overgauw, C.F., ter Horst, H., Dekker, H., Okhuijsen, B., Seynen, M., Vijftigschild, A., Han, P., Katan, A.J., Schoots, K., Schumm, R., van Loo, W., Oosterkamp, T.H., and Frenken, J.W.M. (2005). Scanning probe microscopes go video rate and beyond. *Review of Scientific Instruments*, 76(5), 053710(1–9).

Schitter, G., Åström, K.J., DeMartini, B.E., Thurner, P.J., Turner, K.L., and Hansma, P.K. (2007). Design and modeling of a high-speed AFM-scanner. *IEEE Transactions on Control Systems Technology*, 15(5), 906–915.

Schitter, G., Thurner, P.J., and Hansma, P.K. (2008). Design and input-shaping control of a novel scanner for high-speed atomic force microscopy. *Mechatronics*, 18(5-6), 282–288.

Sebastian, A., Pantazi, A., Moheimani, S.O.R., Pozidis, H., and Eleftheriou, E. (2008). A self servo writing scheme for a MEMS storage device with sub-nanometer precision. In *Proc. IFAC World Congress*, 9241–9247. Seoul, Korea.